Maresca *et al. Energy Mater* 2024;4:400017
DOI: 10.20517/energymater.2023.84

Energy Materials

Article

Open Access

Check for updates

Superior compatibility of silicon nanowire anodes in ionic liquid electrolytes

Giovanna Maresca[1,2,*], Abinaya Sankaran[3], Luigi J. Santa Maria[3], Michela Ottaviani[3,4], Sebastien Fantini[5], Kevin M. Ryan[3], Sergio Brutti[6], Giovanni Battista Appetecchi[1,*]

[1]ENEA, Technologies and Devices for Electrochemical Storage (TERIN-DEC-ACEL), Rome 00123, Italy.
[2]Department of Basic and Applied Sciences of Engineering, La Sapienza University of Rome, Rome 00185, Italy.
[3]Department of Chemical Sciences and Bernal Institute, University of Limerick, Limerick V94 T9PX, Ireland.
[4]Department of Physics, University of Limerick, Limerick V94 T9PX, Ireland.
[5]Solvionic SA, 11 Chemin des Silos, Toulouse 31100, France.
[6]Department of Chemistry, La Sapienza University of Rome, Rome 00185, Italy.

***Correspondence to:** Dr. Giovanna Maresca, Department of Basic and Applied Sciences of Engineering, La Sapienza University of Rome, Piazzale Aldo Moro 5, Rome 00185, Italy. E-mail: giovanna.maresca@uniroma1.it; Dr. Giovanni Battista Appetecchi, ENEA, Technologies and Devices for Electrochemical Storage (TERIN-DEC-ACEL), Via Anguillarese 301, Rome 00123, Italy. E-mail: gianni.appetecchi@enea.it

How to cite this article: Maresca G, Sankaran A, Santa Maria LJ, Ottaviani M, Fantini S, Ryan KM, Brutti S, Appetecchi GB. Superior compatibility of silicon nanowire anodes in ionic liquid electrolytes. *Energy Mater* 2024;4:400017. https://dx.doi.org/10.20517/energymater.2023.84

Received: 24 Oct 2023 **First Decision:** 6 Dec 2023 **Revised:** 14 Dec 2023 **Accepted:** 5 Jan 2024 **Published:** 12 Mar 2024

Academic Editor: Yuping Wu **Copy Editor:** Fangling Lan **Production Editor:** Fangling Lan

Abstract

Silicon nanowire anodes were investigated in lithium-metal cells using different electrolyte formulations based on 1-ethyl-3-methylimidazolium bis(trifluoromethylsulfonyl)imide, 1-ethyl-3-methylimidazolium bis(fluorosulfonyl)imide and *N*-trimethyl-*N*-butyl-ammonium bis(fluoro sulfonyl)imide ionic liquids. The lithium insertion process in the silicon anode was analyzed by cyclic voltammetry measurements, performed at different scan rates and for prolonged cycles, combined with impedance spectroscopy analysis. A galvanostatic charge-discharge cycling test was performed to analyze the electrochemical performances using different types of ionic liquids. A study of the Solid Electrolyte Interphase layer on the silicon nanowire electrode surface was carried out through X-ray photoelectron spectroscopy. In general, the silicon anodes in 1-ethyl-3-methylimidazolium bis(fluorosulfonyl)imide-based electrolytes show very good reversibility, reproducibility, and efficiency in the lithiation process, even at high scan rates, and exhibit a reversible capacity exceeding 1,000 mA h g^{-1} after 2,000 charge-discharge cycles, corresponding to 46% of the initial value.

Keywords: Silicon anodes, ionic liquids, solid electrolyte interphase, XPS analysis, lithium-ion batteries

INTRODUCTION

Lithium-ion batteries (LIBs) have revolutionized the field of energy storage and are widely used in a wide variety of applications, including electric vehicles (EVs). These batteries are known for their high energy density, lightweight design, and long cycle life, making them an ideal choice for powering EVs[1-4]. The thriving EV markets have created a pressing demand for the advancement of high-energy-density storage devices aiming to achieve an energy density of 500 W h kg^{-1} or higher[5]. However, it is important to note that while LIBs have made significant strides in the EV industry, further research and development are underway to enhance their performance, sustainability, and safety[1-4]. For example, extremely fast overcharging could promote lithium (Li) plating, resulting in detrimental effects on battery performance and safety. Moreover, lithium metal can lead to the growth of dendrites, which are conductive filaments capable of penetrating into the separator and causing short circuits, thermal runaway, and even battery fires or explosions. This risk is particularly relevant in EVs, where large numbers of lithium batteries are densely packed together[4-6].

At the system level, several strategies can be used to prevent the spread of thermal runaways, including the construction of fire-resistant casings, the use of high thermal resistance separators, and the setting of thermal barriers between the cells.

At the material level, ensuring the thermal stability of the cell components, such as cathodes, anodes, and electrolytes, can significantly enhance the intrinsic safety of the LIBs. For the cathode, a protective coating can prevent the extended reaction at the cathode-electrolyte interphase, minimizing the risk of side reactions or degradation[5-7]. From the anode side, replacing the lithium metal anode with an alternative material could be an important step for improving battery safety. In this regard, silicon (Si) has gained attention due to its high capacity for energy storage (4,200 mA h g^{-1} for $Li_{22}Si_5$), high abundance (second most abundant element in the Earth's crust), and intermediate discharging potential (about 0.3-0.4 V *vs.* Li^+/Li^0) which can help in preventing Li dendrite formation. However, for accommodating 4.4 Li atoms, which correspond to the $Li_{22}Si_5$ alloy, the Si structure is exposed to detrimental stress induced by a large volume change (about 400%), which can lead to rapid degradation of the electrode and pulverization under prolonged cycling[8-10].

In 2008, Chan *et al.* demonstrated that the nanostructures, particularly nanowires (NWs), can hold a large strain without developing fractures and cracks on the NW surface, securing a good electrical contact between the current collector and the tip of the NW[11]. In addition, the large volume expansion in the Si anode strongly affects the stability of the so-called solid electrolyte interphase (SEI)[8]. The SEI layer forms at the negative electrode during the initial charging process and consists of a complex heterogeneous and structurally disordered passivation layer containing the organic and inorganic species coming from the decomposition of the electrolyte. It acts as a protective barrier, blocking further reactions between the electrolyte and the anode while allowing the transport of Li-ions[12-15]. For the Si-based anodes, the cyclic expansion and contraction of the active material expose the SEI layer to continuous cracks, forming a "fresh" Si surface that interacts with the electrolyte, creating a new SEI layer[16]. This dynamic, uncontrolled, and non-uniform formation of the layer can negatively affect the safety and long-term stability of the cell.

Ensuring a mechanically robust and chemically stable SEI layer can be facilitated by using functional additives in the electrolyte, such as vinylene carbonate (VC) and fluoroethylene carbonate (FEC)[17-19]. Although the SEI layer is essential for the safety and stability of the cell, the understanding of this nature and behavior remains a significant challenge. The nanometric dimension of this layer (10-50 nm thick) makes its characterization challenging and easily biased by artifacts. For example, incomplete electrode

post-mortem cleaning procedures (washing and drying) can leave electrolyte/salt residues, whereas many SEI constituents are particularly sensitive to humidity and air pollution. As an example, ROLi and $ROCO_2Li$ can react with ambient CO_2 to induce *ex-situ* SEI evolution to form large amounts of Li_2CO_3. The SEI formation is affected by multiple factors: current rates, temperature, voltages, electrolyte composition, and concentration. Recently, the use of complementary techniques, including predictive computational models such as machine learning, has been demonstrated successfully to gain insights into the formation and progression of the SEI layer. For the characterization of the surface of the SEI layer, the most common surface analysis techniques are atomic force microscopy (AFM), secondary ion mass spectroscopy (SIMS), and X-ray photoelectron spectroscopy (XPS). Additional information on the morphology of the layer can be obtained using scanning electron microscopy (SEM) and transmission electron microscopy (TEM)[12,13,16,19,20].

Turning back to the safety concerns related to electrolytes, the most radical way to remove this risk is the substitution of flammable organic carbonate-based electrolytes with intrinsically non-flammable ionic liquid (IL) electrolytes. ILs also have the advantages of wide electrochemical stability windows and excellent thermal stability. They consist of salts that are liquid at room temperature because of their loosely connected cation and anion asymmetric structure. Typically, IL electrolytes are formed by quaternary ammonium cations such as imidazolium, pyridinium, pyrrolidinium, piperidinium, and ammonium, coupled with anions (with low Lewis basicity) such as tetrafluoroborate (BF_4^-), hexafluorophosphate (PF_6^-), bis(trifluoromethylsulfonyl)imide ($TFSI^-$), and bis(fluorosulphonyl)imide (FSI^-)[16,19,21,22]. It has been demonstrated that, particularly for the ILs formed by quaternary ammonium cations and TFSI or FSI anions, they are cathodically stable on Si electrodes[23,24]. Notably, FSI-based ILs revealed better cycling behavior and higher capacity retention as compared to the TFSI-based ones in the Si-based electrode, probably due to the formation of a more stable SEI layer[22,25]. The inorganic products coming from the decomposition of FSI-based IL electrolytes (such as LiOH and Li_2O) on the Si anode can promote Li-ion diffusion and boost the cycling performance[22].

In this scenario, this work focused on investigating the lithiation process in Sn-seeded Si NW (hereafter Sn-Si NW) anodes with different binary IL formulations (0.2LiTFSI-0.8EMITFSI (LiTFSI: lithium bis(trifluoromethylsulfonyl)imide; EMITFSI: 1-ethyl-3-methylimidazolium bis(trifluoromethylsulfonyl)imide), 0.2LiTFSI-0.8EMIFSI (EMIFSI: 1-ethyl-3-methylimidazolium bis(fluorosulfonyl)imide), and 0.2LiFSI (LiFSI: lithium bis(fluorosulfonyl)imide)-0.8EMIFSI) with LiTFSI and LiFSI salts. The effect of the FSI and TFSI anions was examined through cyclic voltammetry (CV) and impedance analysis. The modulation of the Li-ion diffusivity across the SEI layer, on which the rate performance of Sn-Si NW anodes depends, was evaluated by analyzing the Li-ion diffusion coefficient. The role of the anions and cations in the cell performance in galvanostatic tests was decoupled by comparing different IL electrolyte formulations (0.2LiFSI-0.8 *N*-trimethyl-*N*-butyl-ammonium bis(fluoro sulfonyl)imide ($N_{1114}FSI$)). Moreover, the effect of the FEC additive was studied for the LiTFSI-EMIFSI electrolyte. Finally, the SEI layer composition was analyzed (*ex-situ* XPS) for the Sn/Si NW electrode after a different number of charge-discharge cycles.

EXPERIMENTAL

The EMITFSI, EMIFSI, and $N_{1114}FSI$ were synthesized and purified according to an eco-friendly route reported elsewhere[26-28]. The ILs were investigated as electrolyte components in (binary) mixtures with LiTFSI (3M, > 99.9 wt.%, battery grade) and LiFSI (Solvionic, 99.9 wt.%) in the Li:IL = 1:4 mole ratio. The 0.2LiTFSI:0.8EMITFSI, 0.2LiTFSI:0.8EMIFSI, 0.2LiFSI:0.8EMIFSI, and 0.2LiFSI:0.8$N_{1114}FSI$ electrolyte formulations were considered for electrochemical characterization in Si-based electrodes. The FEC (Solvionic, > 99 wt.%) was used as an organic additive for optimizing the electrolyte/silicon interface. It was

used in the mole fraction from 0.01 to 0.04 to define the optimal content for the electrolyte formulations. Table 1 summarizes the weight composition of the investigated electrolyte formulations. The 1M Lithium hexafluorophosphate ($LiPF_6$) in Ethylene Carbonate: Dimethyl Carbonate (EC:DC = 1:1 vol.%) with 3 wt.% FEC solution was provided by Solvionic and used for comparison purposes.

Copper silicide ($Cu_{15}Si_4$) NWs were utilized as nanostructured hosts for amorphous silicon (a-Si) deposition; the procedure was already described in detail elsewhere[29,30]. The a-Si anodes have a Si mass loading ranging from 0.1 to 0.25 mg cm^{-2}, corresponding (accounting for a Si theoretical specific capacity equal to 4,200 mA h g^{-1}) to a capacity from 0.42 to 1.05 mA cm^{-2}. The tin-seeded silicon NW (Sn-Si NW) anodes were synthesized in a solvent-vapor system following a method already reported in the literature[31]. The Sn/Si NW anodes present a mass loading between 0.1 and 0.25 mg cm^{-2}, corresponding (accounting for nominal capacity values equal to 2,000 and 994 mA h g^{-1} for Si and Sn, respectively) to an overall capacity from 0.13 to 0.54 mA h cm^{-2}.

The materials used in this work were dried, stored, and handled in an Ar-filled dry box (Jacomex, Dagneux, France, O_2, and H_2O level < 1 ppm).

Electrochemical measurements

The electrochemical measurements were carried out on lithium metal cells using CR2032 coin cells. The lithium metal disk (500 μ thickness, 10 mm diameter) was purchased by Linyi Gelon LIB Co and used as the counter electrode. The a-Si and/or Sn-Si NW anodes were used as working electrodes. The electrodes were separated using two disks of glass fiber (16 mm diameter) separators (Whatman TM, Maidstone, UK). The cells were kept under vacuum for 30 min to allow complete loading of the IL electrolyte into the electrode and the separator.

A preliminary evaluation of the electrochemical processes taking place in Li/Si cells was run in a-Si anodes through cyclic voltammetric (CV) analysis paired with potentiostatic electrochemical impedance spectroscopy (PEIS) measurements. The following electrolyte formulations were used: 0.2LiTFSI:0.8EMITFSI, 0.2LiTFSI:0.8EMIFSI, and 0.2LiFSI:0.8EMIFSI. The CV tests were performed between 0.01 to 2 V *vs.* $Li^+/Li°$ at increasing scan rates, i.e., from 0.05 to 1 mV s^{-1} (four consecutive CV cycles were run at each selected scan rate), followed by 500 cycles at constant scan rate of 1 mV s^{-1}. The PEIS was carried out on the fresh cells and at the end of each increasing scan rate CV family in the 10 kHz-0.1 Hz frequency range with 10 mV amplitude voltage.

Galvanostatic charge-discharge (GC) measurements were carried out on Li/Sn-Si NW cells using 0.2LiTFSI:0.8EMIFSI, 0.2LiFSI:0.8EMIFSI, and 0.2LiFSI:0.8N_{1114}FSI as the electrolytes. The cells were cycled between 0.01 and 2 V *vs.* $Li^+/Li°$ at current rates from 0.1C to 10C.

All the electrochemical tests were carried out in a climate chamber at 20 °C using a Biologic (Seyssinet-Pariset, France) multichannel battery cycler.

Interfacial characterization

XPS was carried out to get information on electrochemical passivation layer (SEI) formation on the Sn-Si NW surface. XPS analysis was performed under an ultra-high vacuum (~10^{-9} mbar) using a Kratos AXIS ULTRA spectrometer with a monochromatic Al Kα X-ray radiation source (hν = 1,486.6 eV). Pass energies of 160 and 20 eV were used for survey spectra and narrow regions, respectively. The C 1s line at 284.8 eV was used as a charge reference. These spectroscopic studies were performed on the Sn-Si NW surface after

Table 1. IL electrolyte formulations investigated with Si anodes

Mole fraction	Lithium salt	Mole fraction	IL	Mole fraction	Additive
0.20	LiTFSI	0.80	EMITFSI	-	-
0.20	LiTFSI	0.80	EMIFSI	-	-
0.20	LiTFSI	0.79	EMIFSI	0.01	FEC
0.20	LiTFSI	0.78	EMIFSI	0.02	FEC
0.20	LiTFSI	0.73	EMIFSI	0.07	FEC
0.20	LiTFSI	0.80	EMIFSI	+ 3 wt.%	FEC
0.20	LiFSI	0.80	EMIFSI	-	-
0.20	LiFSI	0.80	N_{1114}FSI	-	-

electrochemical tests at different states of charge in lithium salt-IL electrolytes: (i) pristine material; (ii) 1 cycle @0.1C; and (iii) 1 cycle @0.1C + 10 cycles @1C. After the cell dismantling, the Si electrodes were rinsed with Tetrahydrofuran (Sigma Aldrich, anhydrous, ≥ 99.9%) at least three times to remove the residual electrolyte, vacuum-dried at room temperature, and then transferred directly to the XPS analysis chamber.

RESULTS AND DISCUSSION

Several electrolyte formulations based on different ILs in combination with the LiTFSI salt have been previously synthesized and characterized in terms of ion transport properties and electrochemical stability[32]. Results summarized in Table 2 show that the EMIFSI-, EMITFSI-, and N_{1114}FSI-based electrolytes are rather promising as electrolyte components in LIB systems, and therefore, they were selected for the electrochemical tests with Si anodes.

Lithium intercalation process

The reversibility of the Li^+ storage process was studied on a-Si anodes in the 0.2LiTFSI-0.8EMITFSI, 0.2LiTFSI-0.8EMIFSI, and 0.2LiFSI-0.8EMIFSI electrolytes through CV tests at different scan rates and for prolonged cycles. The results are displayed in Figure 1. The current value is normalized with respect to the Si electrode mass loading (A g^{-1}).

A broad feature located around 1.2 V *vs.* Li^+/Li was observed during the first cathodic scans in all three cases [Figure 1A-C], which relates to the passivation layer (SEI) formation onto the Si anodes[23,33]. This peak (magnified in Supplementary Figure 1) disappears in the subsequent cycles, suggesting stabilization of the electrode/electrolyte interface. The Li/Si cell with 0.2LiTFSI-0.8EMITFSI shows the peaks relative to the lithiation of a-Si in the first cathodic scan, but no evident peaks can be noticed in the following cycles; this suggests non-optimal SEI formation (instead progressive lithiation of the amorphized Si anode)[23,33], highlighting for large irreversible capacity and, consequently, low initial coulombic efficiency and indicating poor reversibility of the lithium dealloying. The progressive replacement of the TFSI anion with the FSI one in the IL [Figure 1B] and in both IL and lithium salt [Figure 1C] results in very beneficial effect on the cycling behavior. The lithiation of Si initially causes the formation of the amorphous phase Li_xSi, which turns into a crystalline phase below 0.06 V *vs.* Li^+/Li[24], corresponding to two well-defined peaks, located at 0.15 and 0.05 V *vs.* Li^+/Li, as can be observed in Figure 1B and C. In the reverse scan, two similar features around 0.3 and 0.5 V *vs.* Li^+/Li arise from the two-phase reaction from crystalline $Li_{15}Si_4$ to amorphous Li_xSi ($x \approx 2$), followed by the formation of the delithiated amorphous Si[24,34]. This indicates good reversibility of the delithiation process during the anodic scan, i.e., leading to much higher stored and delivered capacity, possibly due to an optimal SEI growth onto the Si electrode, given by the much better film-forming ability of the FSI anion with respect to the TFSI one[23,24]. The complete overlap of the voltammograms, even at high scan rates and for prolonged cycles [Figure 1D and E], suggests good reversibility and high coulombic

Table 2. Summary of ionic conductivity (error bar: 10%) and anodic breakdown voltage (error bar: 0.01 mV) values (*vs.* the Li^+/Li^0 redox couple), determined by CV tests of different ionic liquid electrolytes with the LiTFSI salt (mole fraction equal to 0.2)

IL sample	Conductivity/S cm^{-1}			Voltage (1st scan)/V		Voltage (2nd scan)/V	
	-10 °C	20 °C	50 °C	10 μA cm^{-2}	20 μA cm^{-2}	10 μA cm^{-2}	20 μA cm^{-2}
EMIFSI	1.5×10^{-3}	6.0×10^{-3}	1.3×10^{-2}	4.31	4.68	4.50	4.91
EMITFSI	3.6×10^{-4}	1.4×10^{-3}	3.5×10^{-3}	4.34	4.95	4.66	4.94
N_{1114}FSI	1.6×10^{-4}	1.3×10^{-3}	3.9×10^{-3}	4.23	4.93	4.75	> 5.00
N_{1114}TFSI	5.0×10^{-8}	3.9×10^{-4}	1.9×10^{-3}	4.87	> 5.00	> 5.00	> 5.00
N_{1113}TFSI	$< 1 \times 10^{-9}$	4.1×10^{-5}	3.1×10^{-3}	-	-	-	-
$N_{111(201)}$TFSI	$< 1 \times 10^{-9}$	2.9×10^{-6}	3.8×10^{-3}	-	-	-	-
$N_{122(201)}$TFSI	4.8×10^{-5}	5.6×10^{-4}	1.9×10^{-4}	4.48	4.90	4.84	> 5.00

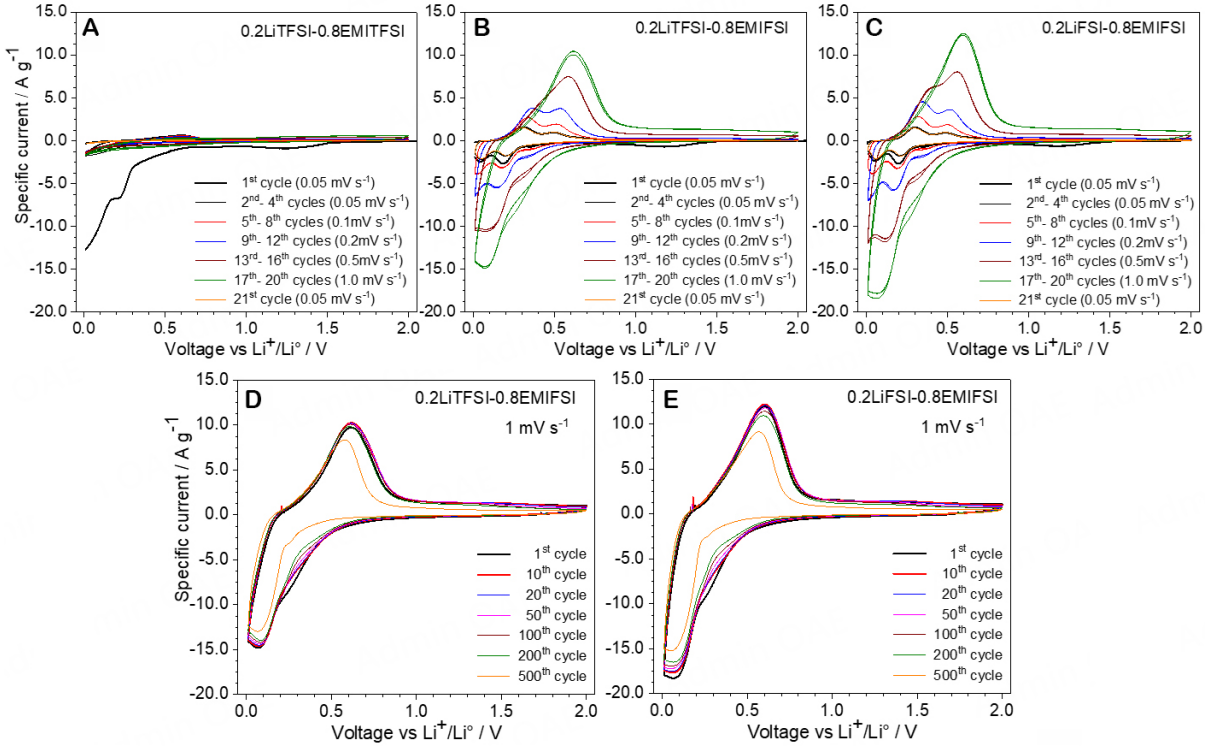

Figure 1. Cyclic voltammetry of Li/Si cells containing 0.2LiTFSI-0.8EMITFSI (A), 0.2LiTFSI-0.8EMIFSI (B), and 0.2LiFSI-0.8EMIFSI (C) electrolytes run at different scan rates and for prolonged cycles with a scan rate of 1 mV s^{-1} carried out on 0.2LiTFSI-0.8EMIFSI (D)- and 0.2LiFSI-0.8EMIFSI (E)-based cells. T = 20 °C.

efficiency of the alloying/dealloying process during cycles in the 0.2LiTFSI-0.8EMIFSI and 0.2LiFSI-0.8EMIFSI electrolytes. The increase of the scan rate results in progressive enhancement of the current flow through the cell, leading to more pronounced and defined current *vs.* voltage features in both verses, with only a moderate shift of the maximum value due to diffusive processes that take place into the electrolyte, according to the Randles-Sevcik equation[35,36]. At 0.2 mV s^{-1}, two distinguished profiles are still observed, both in the cathodic (Li^+ alloying) and anodic (Li^+ dealloying) verse, whereas at faster scan rates, they are not split. Larger values of specific current associated with the electrochemical processes, resulting in higher capacity involved in the (de)lithiation process, were observed in the 0.2LiFSI-0.8EMIFSI cells with respect to the 0.2LiTFSI-0.8EMIFSI ones. Prolonged CVs were run only on 0.2LiTFSI-0.8EMIFSI and 0.2LiFSI-0.8EMIFSI cells after CV tests displayed in Figure 1B and C to investigate the reversibility of the Li^+ alloying

process under hard operative conditions, i.e., 500 cycles at 1 mV s^{-1}. The results, as illustrated in Figure 1D and E, show two defined features around 0.25 and 0.1 V (cathodic scan) and around 0.6 V (anodic scan). A very good reversibility of the lithium alloying process is observed even after 500 cycles, witnessed by the good correspondence between the cathodic and anodic features. A remarkable reproducibility of the CV traces is recorded for the first 200 cycles, whereas progressive, even modest, decrease of the CV profile is observed up to the 500th cycle. To summarize, the 0.2LiFSI-0.8EMIFSI electrolyte exhibits comparable voltammetric features to those of 0.2LiTFSI-0.8EMIFSI; however, it shows evidence of higher capacity decay (i.e., more depleted CV profile) after prolonged CV tests (> 200 cycles).

The mobility of Li-ions at the electrolyte/silicon interface directly depends on the redox reaction rate according to the Randles-Sevcik equation[35,36] and can be modulated by the SEI layer formed onto the silicon particles, which can enhance the rate performances and reduce the lithium trapping[37]. Therefore, the Li-ion diffusion coefficient D_{Li+} (cm^2 s^{-1}) was calculated for a-Si anode cycled into 0.2LiTFSI-0.8EMIFSI and 0.2LiFSI-0.8EMIFSI electrolytes, evaluating the CV tests recorded at different scan rate [Figure 1B and C] described in the previous paragraph. The D_{Li+} was calculated based on the Randles-Sevcik equation (Equation 1)[38,39] for a semi-infinite diffusion of Li-ions:

$$Ip = 0.4463\ n\ FAC\ (nFvD_{Li+}/RT)^{1/2} \quad (1)$$

where the I_p is the peak current, and R, F, and T are the gas constant, Faraday constant, and temperature (K), respectively. A (cm^2) is the active surface area of the a-Si anode, n is the number of electrons in the reaction, C (mol cm^{-3}) is the Li_+-ion concentration in the electrolyte, and v (V s^{-1}) is the scan rate. The relationship of the cathodic and anodic current peaks (I_c and I_a) with the square root of the scan rate is reported in Figure 2. The current peaks in anodic A_n and cathodic C_n scan, taken into consideration for the evaluation of D_{Li+}, are displayed in Supplementary Figure 2. The slope of the linear fit [Supplementary Figure 3] between I_p and $v^{0.5}$ was used to estimate the D_{Li+}[40-42]. Both systems show a linear behavior, meaning the diffusion-controlled reaction[43] and a peak current ratio (I_{pa}/I_{pc}) ≈ 1, suggesting reversible lithiation process and no parasitic reaction associated with the electron transfer[39]. The D_{Li+} was found to be equal to (9.6 ± 0.5) × 10^{-10} cm^2 s^{-1} for 0.2LiTFSI-0.8EMIFSI and (2.5 ± 0.1) × 10^{-10} cm^2 s^{-1} for 0.2LiFSI-0.8EMIFSI electrolytes, comparable with the results reported in the literature for Li_xSi phases in organic electrolytes and obtained through different techniques[44,45]. The error related to the D values is equal to 5%.

Impedance measurements

Impedance measurements were conducted after each CV family test run at different scan rates [Figure 1] and reported in Supplementary Figure 4 as Nyquist plots. The impedance responses display a semicircle pattern at medium-high frequencies and a straight line at low frequencies, in agreement with other studies on similar anode materials in IL electrolytes[43,46]. The high-frequency intercept with the real axis corresponds to the bulk resistance (R_{bulk}) of the IL[47-49], and the semicircle diameter gives the overall interfacial resistance R_{int} [47-49]. Figure 3 plots the dependence of R_{bulk} (A) and R_{int} (B), determined from the impedance responses [Supplementary Figure 4] taken [in open circuit voltage (OCV) conditions] after each CV family of Figure 1, as a function of the scan rate. The resistance values summarized in Table 3 were evaluated through the equivalent circuit models depicted in Supplementary Figure 5, where Q_{dl} is the constant phase element taking into account the double layer capacitance, and C_l is the electrode limit capacitance[47-49]. R_{bulk} values equal to 1.7, 1.6, and 1.3 Ω cm were detected (at 20 °C) for the 0.2LiTFSI-0.8EMITFSI, 0.2LiTFSI-0.8EMIFSI, and 0.2LiFSI-0.8EMIFSI cells, respectively, i.e., close to those reported in previous work and summarized in Table 2[32]. Significantly, no change of R_{bulk} is observed during the CV

Table 3. R_{bulk} (Ω cm) and R_{int} (Ω cm^2) parameters, associated with Li/a-Si cells containing the 0.2LiTFSI-0.8EMITFSI, 0.2LiTFSI-0.8EMIFSI, and 0.2LiFSI-0.8EMIFSI electrolytes, determined in OCV conditions after CV tests run at increasing scan rates. T = 20 °C

Scan rate/mVs $^{-1}$		Pristine	0.05	0.1	0.2	0.5	1
0.2LiTFSI-0.8EMITFSI	R_{bulk}	1.7 ± 0.2	3.2 ± 0.3	5.8 ± 0.6	5.8 ± 0.6	6.3 ± 0.6	6.1 ± 0.6
	R_{int}	-	200 ± 20	230 ± 20	250 ± 30	250 ± 30	250 ± 30
0.2LiTFSI-0.8EMIFSI	R_{bulk}	1.6 ± 0.2	0.9 ± 0.1	1.5 ± 0.2	1.6 ± 0.2	1.7 ± 0.2	1.6 ± 0.2
	R_{int}	-	65 ± 6	39 ± 4	37 ± 4	33 ± 3	35 ± 3
0.2LiFSI-0.8EMIFSI	R_{bulk}	1.3 ± 0.1	0.8 ± 0.1	1.3 ± 0.1	1.3 ± 0.1	1.3 ± 0.1	1.3 ± 0.1
	R_{int}	-	30 ± 3	18 ± 2	18 ± 2	18 ± 2	18 ± 2

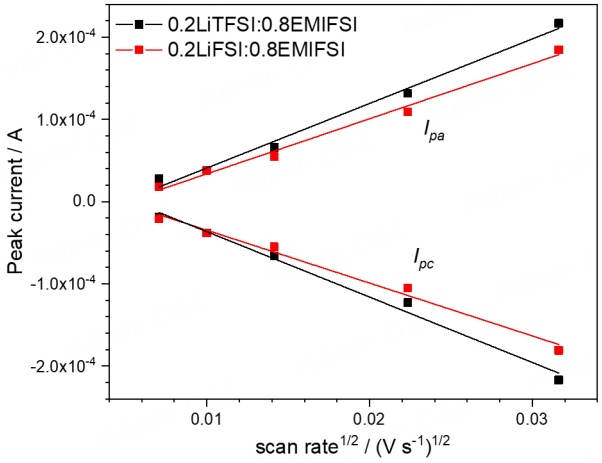

Figure 2. Linear fits for the anodic and cathodic peak currents versus square root of the scanning rates of a-Si electrodes using 0.2LiTFSI-0.8EMIFSI and 0.2LiFSI-0.8EMIFSI electrolytes. T = 20 °C.

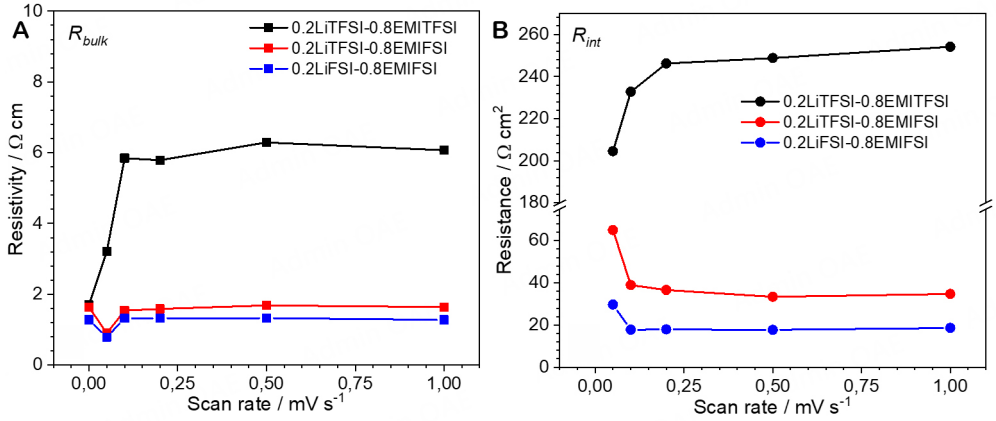

Figure 3. Evolution of the electrolyte R_{bulk} (A) and overall interfacial R_{int} (B) resistance during CV tests run at different scan rates for Li/a-Si cells in 0.2LiTFSI-0.8EMIFSI and 0.2LiFSI-0.8EMIFSI. T = 20 °C.

tests, confirming the good electrochemical stability of the IL-based electrolytes and the negligible lithium depletion from the electrolyte. However, the replacement of the TFSI anion with FSI results in a sharp decrease of R_{int}. For instance, more than 200 Ω cm^2 are recorded for the 0.2LiTFSI-0.8EMITFSI cells [Supplementary Figure 4A], whereas only 40 and 20 Ω cm^2 are approximately exhibited by those with 0.2LiTFSI-0.8EMIFSI [Supplementary Figure 4B] and 0.2LiFSI-0.8EMIFSI [Supplementary Figure 4C],

respectively. These results, in very good agreement with the voltammetry data of Figure 1, indicate large decrease in interfacial resistance accompanying the transformation of the original discrete a-Si into a stable porous network (nano-ligaments)[23,33]. Once more, it highlighted the beneficial effect of the FSI anion at the interface with the Si electrode, playing a key role in the SEI composition and, therefore, the active material morphology. For instance, a suitable SEI layer leads to a larger surface area offered for the alloying process by the a-Si network and to the accommodation of more facile charge transfer at the electrode/electrolyte interface. Conversely, the TFSI anion is not able to promote the growing-up of suitable SEI, leading to poor Li^+ alloying and, therefore, low performance. This issue is in good agreement with both the CV results of Figure 1. The impedance response recorded after 500 cycles (shown in Supplementary Figure 4D and E) exhibits similar shape with respect to that of the Nyquist plots of the first family cycles [Supplementary Figure 4B and C]. No practical change of R_{bulk} is observed, whereas a more slightly depressed semicircle is exhibited by the 0.2LiFSI-0.8EMIFSI cells, nevertheless demonstrating the electrochemical reliability of the 0.2LiTFSI-0.8EMIFSI and 0.2LiFSI-0.8EMIFSI electrolytes. An overall interfacial resistance lower than 100 Ω cm^2 is recorded in both electrolyte formulations. To summarize, the a-Si anodes seem to show comparable behavior in both 0.2LiTFSI-0.8EMIFSI and 0.2LiFSI-0.8EMIFSI.

Cycling behavior

The CV investigation on a-Si anodes has shown how EMIFSI is a more appropriate IL solvent compared to EMITFSI for Si electrodes. Therefore, this IL was used as the electrolyte component for further investigations on Sn-Si NW anodes. The N_{1114}FSI IL was employed for comparison purposes. The performances in Li-metal cells of Sn-Si NW anodes were estimated by galvanostatic cycling measurements. Preliminary examinations [Supplementary Figure 6] have evidenced good and reproducible cycling behavior for a Si:Sn weight ratio above 2.6:1. As a consequence, only anode samples satisfying this parameter were subjected to cycling tests.

Effect of anion and cation

The voltage-capacity profile of the 1st charge-discharge cycle for Sn-Si NW electrodes in EMIFSI and N_{1114}FSI electrolytes is reported in Figure 4A. A series of features, between 1.2 and 0.2 V, can be noticed during the first discharge curve at 0.1C, likely due to the IL electrolyte degradation leading to SEI layer formation onto the electrode surface[23,33]. These features are followed by two plateaus located around 0.25 and 0.15 V, ascribable to the lithiation process. The value of the initial coulombic efficiency (η) and the nominal capacities (Q) delivered during the rate capability tests on Li/Sn-Si NW cells are reported in Table 4. The 0.2LiFSI-0.8EMIFSI cell shows the lowest initial irreversible capacity (Q_{irr}), amounting to 28%, with respect to 0.2LiTFSI-0.8EMIFSI and 0.2LiFSI-0.8N_{1114}FSI cells, which show Q_{irr} equal to 55% and 35%, respectively, but quickly leveling to 99% in all cases, as can be seen in Figure 4A. A stable capacity value is observed in all electrochemical formulations up to 100 cycles, even at very high rates (10C). Higher capacity values were delivered by the 0.2LiFSI-0.8EMIFSI cells at different scan rates, with a gain of ~550 mA h g^{-1} up to 1C and of ~800 mA h g^{-1} at higher current rates (> 2C) with respect to the other electrolyte systems investigated. The LiFSI-EMIFSI cell can deliver above 50% (1,300 mA h g^{-1}) of the nominal capacity at 10 C; meanwhile, the 0.2LiTFSI-0.8EMIFSI and 0.2LiFSI-0.8N_{1114}FSI cells deliver less than 29% and 16%, respectively, of their nominal capacity at the same current rate. The 0.2LiTFSI-0.8EMIFSI and 0.2LiFSI-0.8N_{1114}FSI electrolyte formulations show very similar capacity values which, at high rates (> 1C), slightly decay for the N_{1114}FSI cells, likely due to the faster ion transport properties of the EMIFSI IL with respect to N_{114}FSI[32]. The best performances of the full-FSI cell configuration, in agreement with the CV results, are attributable to the better film-forming ability of the FSI anion with respect to TFSI[23,24]. Conversely, the N_{1114}FSI IL displays lower compatibility towards Sn-Si NW anodes than EMIFSI. Supplementary Figure 7 displays the voltage *vs.* capacity profile of Sn-Si NW anodes in different electrolyte formulations at increasing scan rates. The voltage of Si alloying plateaus is distributed around 0.1 V, and the dealloying

Table 4. Initial Coulombic efficiency (η) and reversible capacity, delivered at different scan rates, of Li/Sn-Si NW cells in different electrolyte formulations

Electrolyte mixture	1st cycle η/%	Q/mA h g^{-1}							
		0.1C	0.2C	0.5C	1C	2C	5C	10C	$1C_{100th}$
0.2LiTFSI-0.8EMIFSI	45	1,995	1,918	1,774	1,611	1,363	904	586	1,622
0.2LiFSI-0.8EMIFSI	72	2,522	2,442	2,317	2,175	2,006	1,720	1,313	2,027
0.2LiFSI-0.8 N_{1114}FSI	65	1,998	1,905	1,715	1,512	1,226	731	414	1,494

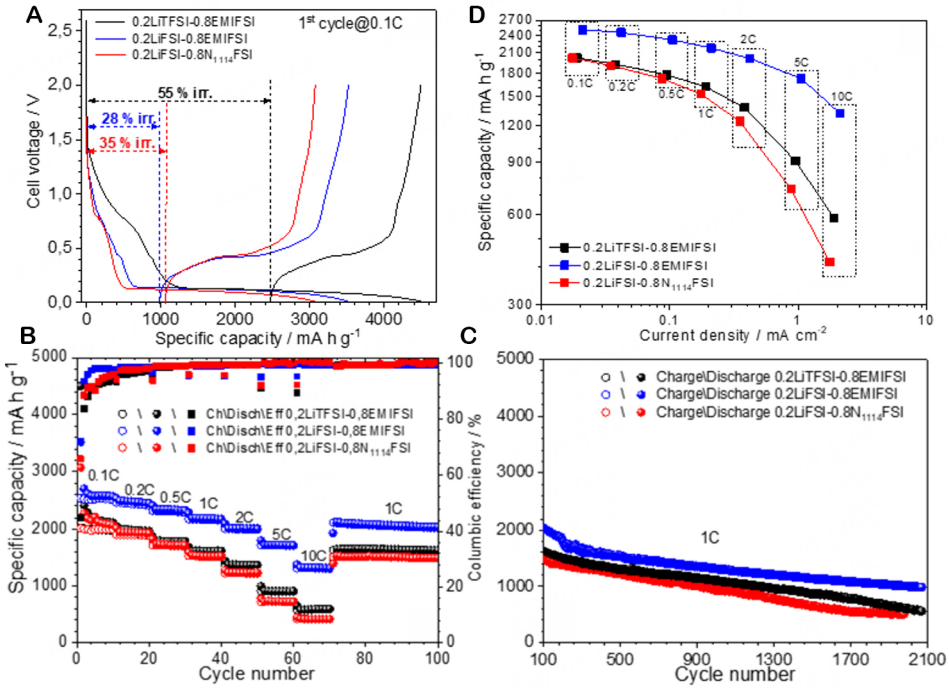

Figure 4. 1st discharge-charge curves (A), cycling performance at different rates (B and C), and reversible capacity *vs.* current density dependence (D) of Li/Si cells in 0.2LiTFSI-0.8EMIFSI, 0.2LiFSI-0.8EMIFSI, and 0.2LiFSI-0.8N_{1114}FSI electrolytes. The cycling behavior of Li/Si cells in organic electrolytes (1M $LiPF_6$ in EC:DMC 1:1 v:v 3 wt.% FEC) is reported for comparison purposes. T = 20 °C.

plateaus are at about 0.4 V, as reported in the literature[34,50,51]. The presence of Sn in the working electrode is evidenced by the two less-defined plateaus in the potential range of 0.45-0.6V [Supplementary Figure 7], attributable to the two-phase alloying reaction that involved the formation of the dominant phases Li_2Sn_5 and LiSn[34,51]. The increase of the current rate from 0.1C to 5C does not result in significant qualitative change of the voltage profile shape, but it does lead to an increase of lithiation/de-lithiation plateau slope attributed (and to an increase in ohmic drop) to diffusive phenomena within the IL electrolyte, especially at high rates. The rate capability tests [Figure 4B] were followed by prolonged tests run at 1C [Figure 4C] and have shown a capacity recovery up to the starting value at 1C. Very interesting capacity retention, despite a decay observed after 100 cycles, is generally exhibited by these electrolyte formulations; i.e., 1,005 (0.2LiFSI-0.8EMIFSI cells), 608 (0.2LiTFSI-0.8EMIFSI), and 509 (0.2LiFSI-0.8N_{114}FSI) mA h g^{-1} are still delivered after 2,000 consecutive charge-discharge cycles (1C) at 100% of DoD, corresponding to 46% (capacity fading equal to 0.027 per cycle), 37% (0.031% per cycle), and 33% (0.034% per cycle) of the initial capacity discharged at 1C. The remarkably enhanced performances of the 0.2LiFSI-0.8EMIFSI electrolyte, comparable to or overcoming those observed in alkyl carbonate and other IL electrolytes[23,33], are once more likely ascribed to the better film-forming ability of the FSI anion, in combination with the transport properties of the EMI cation. The reversible (charge) capacity *vs.* current density dependence of the Li/Sn-Si

NW Sn cells [Figure 4D] evidences a lower rate region, where the capacity is limited by the diffusion phenomena taking place within the Si electrode[52,53], distinguished by the higher rate one characterized by a more pronounced slope of the capacity *vs*. current density curve due to diffusive phenomena occurring in the IL electrolyte[52,53]. The lower rate region limit is around 0.3 mA cm^{-2} for the 0.2LiTFSI-0.8EMIFSI and 0.2LiFSI-0.8N114FSI electrolytes: above this current rate, the electrochemical behavior of the Li/Si cells is governed by diffusive phenomena. Interestingly, the lower rate region extends up to 1 mA cm^{-2} in 0.2LiFSI-0.8EMIFSI cells, indicating that diffusion processes become predominant in this electrolyte at much higher current density with respect to that observed in 0.2LiTFSI-0.8EMIFSI and 0.2LiFSI-0.8N_{114}FSI. To summarize, the 0.2LiFSI-0.8EMIFSI electrolyte exhibits, among the investigated IL formulations, the best cyclic behavior in Sn-Si NW anodes.

Effect of FEC organic additive content

The Sn-Si NW anodes have also been studied in the presence of FEC organic additives to investigate a possible improvement of the electrolyte/electrode interface[17]. The GC tests, as reported in Figure 5, were carried out in LiTFSI-EMIFSI electrolytes containing different FEC molar fractions (summarized in Table 1). The first discharge profile at 0.1C [Figure 5A] exhibits the features already discussed in the previous paragraph; however, the progressively increasing FEC content is seen to enhance the features located in the 1.7-0.2 V range and ascribable to irreversible electrolyte decomposition. In particular, at FEC content equal to 3 wt.%, a very wide plateau is observed around 0.4 V, leading to much larger irreversible capacity. The reversible nominal capacity, the initial coulombic efficiency (i.e., from 45% to 55%), and the cycling behavior (even at 10C) up to about 100 cycles are seen slightly increasing (i.e., from 2,000 to about 2,100 mA h g^{-1}) after incorporation of a FEC mole fraction equal to 0.01, which exhibits at 1C and 10C a delivered capacity of 1,800 and 750 mA h g^{-1} (*vs*. 1,650 and 450 mA h g^{-1} of the FEC-free cells), respectively. Further increases of the FEC up to 3 wt.% content lead to decreased performance. The nominal capacity and the coulombic efficiency fall down to 1,500 mA h g^{-1} and 14%, respectively. Therefore, the presence of a FEC mole fraction > 0.01 in IL electrolytes seems to support larger consumption of electrolytes and/or hinder the formation of an optimal SEI onto the Sn-Si NW surface. As reported in the literature[54,55], the uncoordinated FEC can passivate the anode surface by forming LiF, which can undergo the formation of HF in the presence of small amount of water, causing the dissolution of the SEI on the Si anode surface. However, more prolonged discharge-charge tests (C) reveal progressive decay in performance. For instance, after 1,000 cycles, the 0.01 FEC cells exhibit lower capacities (950 mA h g-1) than those delivered by the FEC-free ones (1,200 mA h g-1), even approaching the values (900 mA h g-1) shown by the 0.07 FEC and 3 wt.% FEC cells (i.e., no practical difference is seen for FEC mole fractions exceeding 0.07). This means an increase in capacity fading from 0.03% (FEC-free cells) to 0.05% per cycle.

XPS analysis on Sn-Si NW anode surface

To get insight into the SEI layer composition formed on the Sn-Si NW anodes, *ex-situ* XPS analysis was carried out on pristine electrodes after the first charge-discharge cycle and several cycles (reported in Supplementary Figure 8). In order to avoid the binding energy (BE) shifts associated with charging phenomena and to gain good accuracy of the peak assignments, the XPS spectra were collected in the delithiated state. The atomic concentrations of the post-mortem Sn-Si NW anodes are summarized in Table 5 (the pristine electrode is reported for comparison). The SEI layer of the Si electrodes cycled in FEC-based and 0.2LiTFSI-0.8EMIFSI electrolytes exhibits high concentration of fluorine and a bit lower oxygen concentration in conjunction with higher silicon concentration onto the anode surface after several cycles, suggesting thinner passive layer onto a Si electrode, as previously reported in literature[56,57]. Otherwise, the Si anodes in 0.2LiFSI-0.8EMIFSI and 0.2LiFSI-0.8N_{1114}FSI show high sulfur concentrations, which depend on the degradation products of the LiFSI salt[55].

Table 5. Surface composition (atom percentage) of pristine and cycled Sn-Si NW electrodes

		O 1s	C 1s	N 1s	F 1s	S 2p	Si 2p	Li 1s	P 2p
Pristine		14.8	56.3	-	-	-	28.0	-	-
0.2LiTFSI-0.8EMITFSI	1st cycle	31.2	33.0	1.5	4.0	1.1	2.2	26.6	-
	10th cycle	27.9	32.4	3.9	8.2	2.4	0.9	23.8	
0.2LiFSI-0.8EMIFSI	1st cycle	31.1	33.1	3.4	2.0	5.2	0.9	24.0	-
	10th cycle	31.5	31.7	3.7	2.1	5.5	1.3	24.3	
0.2LiFSI-0.8 N_{1114}FSI	1st cycle	30.0	30.8	3.8	3.8	7.3	2.0	21.9	-
	10th cycle	31.2	29.7	3.6	3.1	6.7	0.9	24.6	
0.2LiFSI-0.8EMIFSI + 3 wt.% FEC	1st cycle	28.5	36.7	4.4	4.6	4.0	1.6	20.0	-
	10th cycle	30.7	33.0	2.8	5.6	2.6	0.5	24.6	-
1M $LiPF_6$ in EC:DMC 1:1 v:v + 3 wt.% FEC	1st cycle	31.6	29.6	-	5.9	0.3	1.2	30.8	0.1
	10th cycle	29.5	30.6	-	6.8	0.2	1.4	31.3	0.1

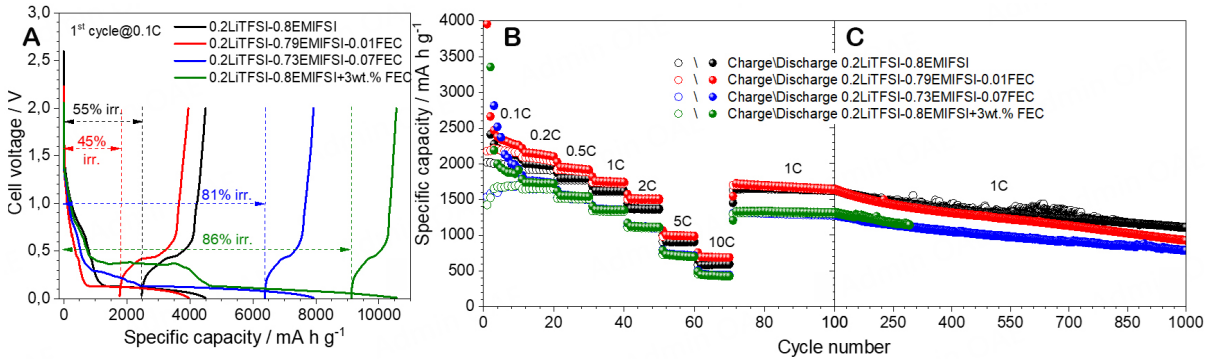

Figure 5. 1st discharge-charge curves (A) and cycling performance at different rates (B and C) of Li/Sn-Si NW cells in LiTFSI-EMIFSI electrolytes with different FEC contents. T = 20 °C.

High-resolution XPS spectra of C 1s, Si 2p, F 1s, Li 1s, S 2p, O 1s, and N 1s, collected for each sample after the first charge-discharge cycles, are displayed in Supplementary Figures 9 and 10, whereas those taken after several cycles are given in Figures 5 and 6. The Si 2p spectra of pristine Sn-Si NW anodes exhibit a narrow feature at 99.8 eV corresponding to the bulk silicon, and the presence of silicon oxides is observed at 100.5 and 102.5 eV[56,58], also confirmed by the O 1s spectra at 532.4 eV[56,58].

The N 1s XPS region of the Sn-Si NW [Figure 6] electrodes, cycled in IL electrolytes, displayed three well-separated peaks: the first two are related to the cation (-C-N-, N^+), i.e., EMI^+ (401.5 eV) and N^+_{1114} (402.6 eV)[59,60], and the anion, which appears around 400 eV (C-N, N-SO) for both $TFSI^-$ and FSI^-[55,61]. The presence of the IL signals is probably due to the caught IL in the porous structure of the Si anodes[62]. The last peak at 398.5 eV is ascribable to Li_3N/LiC_xH_yN or -N=C- double bond in a polymeric network[63-66]. These compounds are associated with the reduction of the electrolyte, which gave place to graphitic carbon[62], evidenced in C 1s spectra [Figure 6] with the sp2 graphitic carbon feature at 284.8 eV. The relative atomic concentration increases upon cycles for the all-TFSI-based electrolyte, decreases for LiFSI-N_{1114}FSI and LiFSI-EMIFSI + 3 wt.% FEC, and finally remains unchanged in LiFSI-EMIFSI, suggesting the growing-up of a stable Li_3N/LiC_xH_yN polymeric network during the first cycle.

The high-resolution XPS spectra of C 1s [Figure 6] display four main features centered around 284.8, 286.1, 288.5, and 289.5 eV in all cases, associated with C-C/C=C[55,67], C-O/C-N[64,68,69], O-C=O/C-F, and CO_3^{2-}[55,67,70]

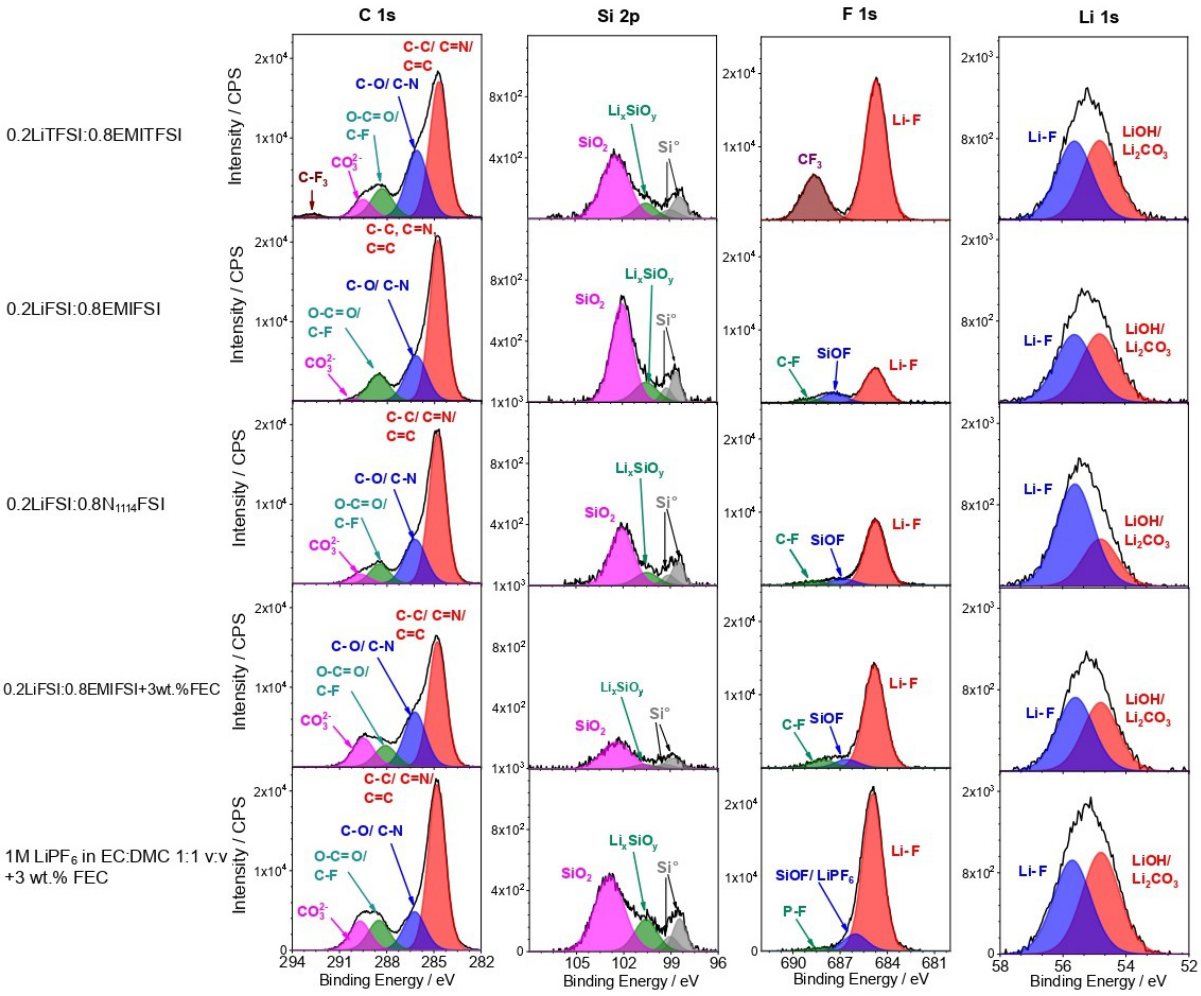

Figure 6. High-resolution C 1s, Si 2p, F 1s, and Li 1s core level spectra obtained on the Sn-Si NW anodes after consecutive lithiation/delithiation steps in different electrolyte formulations (see legend).

species, respectively. The C-C/C=C, C-O/C-N, and CF groups arise from the decomposition of IL (i.e., EMI^+, N_{1114}^+, $TFSI^-$, and FSI^-). For Si-based electrodes cycled in LiTFSI-EMITFSI, the C 1s spectra show a very small peak at 293 eV associated with the CF_3 group[59,61] derived by the TFSI anion, also confirmed by the well-pronounced peak at 688.6 eV in the F 1s XPS spectra [Figure 6]. The CO_3^{2-} can be assigned to Li-$OCOOC_2H_5$ and/or Li_2CO_3 arising from FEC degradation[59] but also from salt decomposition, as was demonstrated in other works[63,71]. The presence of this compound was also detected in the Li 1s spectra at 54.7 eV. This peak is more prominent in FEC-based electrolytes and in LiTFSI-EMITFSI. The area ratio of $C_{286.1}/C_{288.5}$ does not substantially change for LiFSI-EMIFSI and organic electrolytes during cycling, indicating the growth-up of stable SEI during the first cycle. The C 1s spectra of the Sn-Si NW cycled in organic electrolytes reveal quite similar features to those detected in ILs, as already reported in the previous paper[62].

The deconvolution of O 1s spectra [Figure 7] highlights the presence of carbonate species, already observed in the C 1s spectra and evidenced around 532 eV[55,72]. Lithium silicate species (i.e., Li_xSiO_y), related to the lithiation of Si oxide[56,58,73], can be attributed to the peak at 531 eV, which are visible also in the Si 2p spectra at 100.5 eV[55,72]. As described in detail elsewhere[74-76], the broad peak at 533.6 eV, ascribable to O-C=O

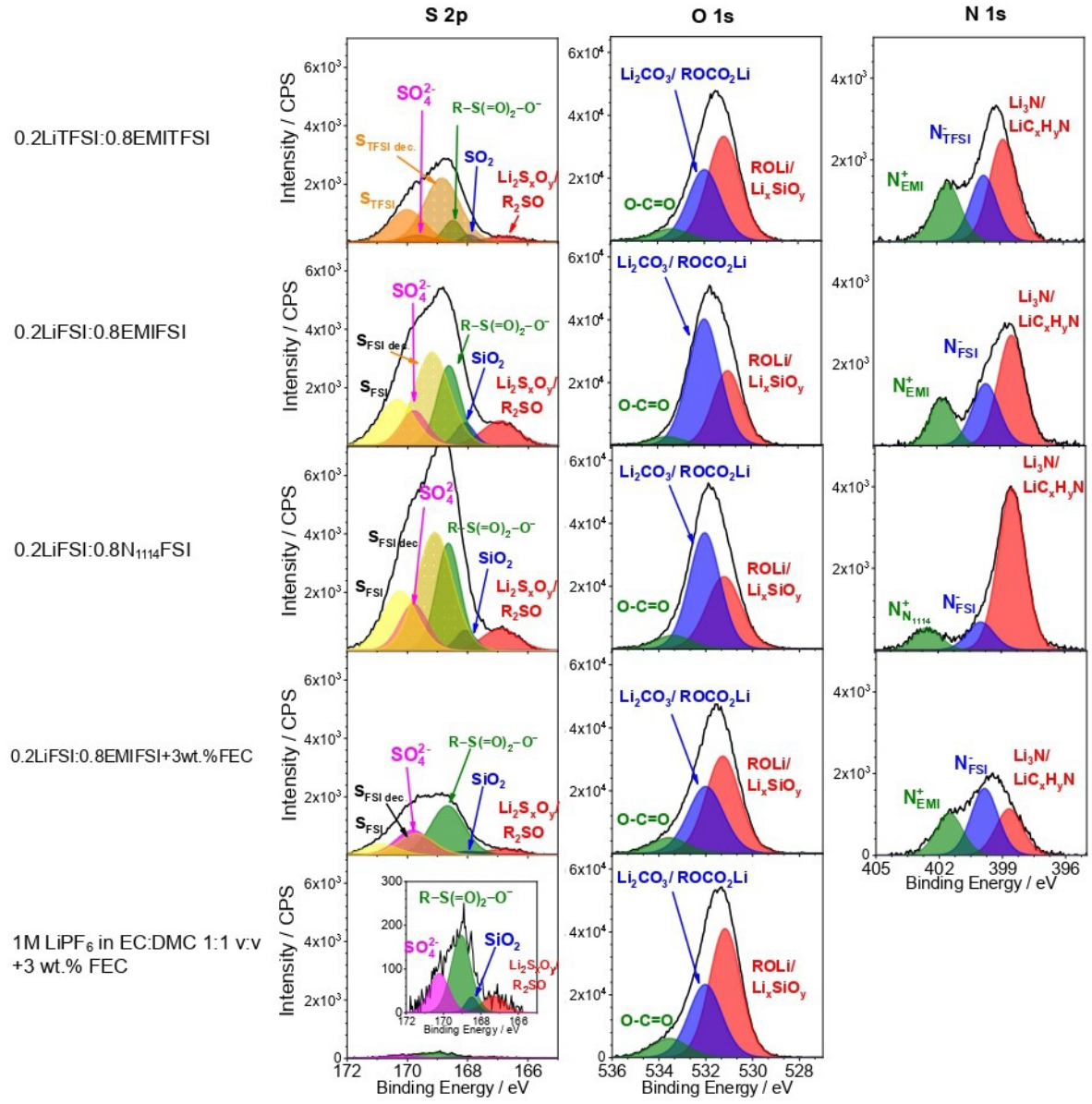

Figure 7. High-resolution S 2p, O 1s, and N 1s core level spectra obtained on pristine Sn-Si NW anodes and after consecutive lithiation/delithiation steps in different electrolyte formulations (see legend).

species, depends on solvent and/or additive polymerization, and it was also observed in the C 1s spectra at 286.1 eV. In all electrolytes, the Si surface is rich in carbonate species, as confirmed by the features in the C 1s and O 1s spectra [Figures 6 and 7].

A large LiF peak at 684.8 eV[55,77] can be observed in the F 1s spectra, in agreement with the Li 1s spectra at 55.6 eV[55,77], due to decomposition of salt (LiTFSI, LiFSI, and $LiPF_6$) by electrochemical reduction of S-F bonds[58] and, during cycling, it can be observed that TFSI-based and FEC-based electrolytes exhibit a higher amount of LiF. As described by Piper *et al.*, FSI^- and $TFSI^-$ are subject to a quite different reduction process, where the FSI^- rapidly releases F^-, forming LiF and SO_2, which suggests the formation of SEI rich in small inorganic compounds[60]. Conversely, $TFSI^-$ can form different products, such as $-SO_2CF_3$. The $-SO_2$ species can also be observed at 168.8 eV in the S 2p spectra, where results are more prominent in the FSI-based

systems. The fast release of F^- and SO_2 may be correlated to the high cycling performance shown by Si-Si NW anodes in LiFSI-EMIFSI electrolytes. This speculation derived from modeling studies performed on the FEC system[78], demonstrating its ability to rapidly release F^- (to form LiF) during its decomposition. The SiOF signal at 686.8 eV corresponds to the Si substrate, indicating the thickness of the SEI layer: in organic electrolytes, it might be covered by the $LiPF_6$ signal, resulting from incomplete removal during the electrode rinsing and/or from intermediate decomposition products with similar BE to $LiPF_6$[76,79]. This feature is more pronounced in LiFSI-EMIFSI and organic (1M $LiPF_6$ in EC:DMC 1:1 v:v + 3 wt.% FEC) electrolytes, indicating thinner SEI on the Si surface. The presence of residual lithium salts (LiTFSI, LiFSI, and $LiPF_6$) and/or their incomplete decomposition products is detected around 688 eV[58,77]. In the case of LiTFSI, it is completely overlapped by the CF_3 signal at 688.6 eV, and the SiOF is not visible.

The S 2p deconvolution [Figure 7] results in a pretty complex spectrum for the Si anode cycled in IL-based electrolytes. It can be divided into three main components. The first one was represented by the $Sp_{3/2}$ peak, which confirms the presence of residual LiTFSI and/or LiFSI salt at 168.8 and 169.1 eV[77], respectively. However, the second one encloses several features, in the range between 169.8 and 168 eV, due to degradation products of imide-based salts that might be assigned to S=O bonds[77,80]. The last weak component, at around 167 eV, is also related to the reduction of Li-imide salt, but this process can also be induced by the X-ray beam[55,76]. The s 2p spectra display very weak peaks, probably due to residual traces of electrolytes.

The Si 2p spectra show the peak related to the bulk silicon at ~98 and ~99 eV[55,56], which, in the case of LiFSI-EMIFSI, tends to increase, meaning a reduction of the SEI layer thickness and in agreement with the results from impedance measurements discussed in Paragraph 3.2. A signal at 100.5 eV can be attributed to Li_xSiO_y, as already previously described, and the last peak at 102.8 eV is associated with the SiO_2 species.

The XPS results suggest a bilayer SEI onto the Si surface, i.e., an outer part composed of organic compounds within a polymeric network that can provide flexibility and good mechanical stability against the volume changes during the Si cycling, and an inner layer dominated by inorganic compounds such as Li_3N and LiF, delivering high Li-ion conductivity, and a graphitic network that provides electronic conductivity[62,63,71]. The different cycling performances can be due to the different densities and porosity of the SEI on the Si surface. The SEI layer onto the Si anodes cycled in LiFSI-EMIFSI and organic electrolytes may be rich in stable LiF and -Si-F compounds which, thanks to their high bonding energy, do not decompose during cycling and promote stable interface with the electrolyte[81,82]. Although, in the other case, the surface layer can contain less stable compounds, such as metastable and less dense, linear alkyl carbonates [-Si-$OCH_2CH_2OCO_2Li$, -Si-$CH_2CH_2OCO_2Li$, $R(OCO_2Li)_2$] and, due to their low bonding energy, can continue to decompose upon cycling, thus feeding irreversible redox reactions that promote silicon dendritization and pulverization, as has been shown by Bongiorno *et al.* The low density of the SEI layer allows the transition of the electrolyte during the Li^+ insertion, which causes the breakup of the -Si-Si- network bond, giving rise to porous structures and cracking[83].

CONCLUSIONS

The lithiation process of Sn-Si NW anodes in different IL electrolyte formulations was investigated through electrochemical and XPS measurements. High reversibility and reproducibility of the Li^+-allowing process are observed for 0.2LiTFSI-0.8EMIFSI and 0.2LiFSI-0.8EMIFSI electrolyte systems through CV analysis carried out at increasing scan rates and for prolonged cycles. Conversely, the full-TFSI electrolytes do not show evident features related to the electrochemical processes, meaning poor reversibility of the lithiation process. The full-FSI cells display higher specific current even after prolonged CV tests (> 200 cycles), indicating larger charge amount involved in the lithiation process.

The Li^+ diffusion coefficient (D_{Li+}), evaluated using the Randles-Savcik equation, is found to be equal to $(9.6 \pm 0.5) \times 10^{-10}$ cm^2 s^{-1} and $(2.5 \pm 0.1) \times 10^{-10}$ cm^2 s^{-1} in the 0.2LiTFSI-0.8EMIFSI and 0.2LiFSI-0.8EMIFSI electrolytes, respectively. These results are consistent with those reported in the literature for organic electrolytes.

The interfacial properties of Li/Si cells were investigated by impedance spectroscopy analysis combined with CV tests. A stable bulk resistance is recorded during CV tests, confirming the good electrochemical stability of the IL-based electrolytes. However, marked improvement in interfacial resistance is observed after replacing the TFSI anion with the FSI. These results, in agreement with the CV tests, are ascribable to the good film-forming ability of the FSI anion.

A reversible capacity exceeding 1,000 mA h g^{-1} is delivered after 2,000 charge-discharge cycles at 1C, corresponding to 46% of the initial value. LiFSI-based electrolytes are seen to behave better compared to those containing LiTFSI. The electrode performances of Sn-Si NW anodes are seen to increase with the Si:Sn weight ratio: for instance, when passing from a Si:Sn ratio of 2.17 to 2.68, 2,400 mA h g^{-1} (about 89% of the nominal capacity = 2,700 mA h g-1) is still delivered at 1C, and 1,000 mA h g^{-1} is even exhibited at 10C (4 mA cm^{-2}). These represent some of the best, if not the best, results observed till now for Si anodes in IL electrolytes. A moderate increase in capacity is observed in the presence of modest contents (0.01 as the mole fraction) of FEC; further addition of FEC, however, does result in performance decay.

A SEI layer, externally composed of a polymeric network and a graphitic network inside, on the Sn-Si NW anode surface was revealed by XPS analysis. The supposed high density of the SEI layer, which hinders the crack formation on the Si surface in the case of 0.2LiFSI-0.8EMIFSI and organic (1M $LiPF_6$ in EC:DMC 1:1 v:v + 3 wt.% FEC) electrolytes, can support for the better cycling behavior.

To summarize, the 0.2LiFSI-0.8EMIFSI electrolyte has shown very high compatibility and excellent battery behavior in lithium cells with Sn-Si NW anodes, and therefore, it can be considered a very appealing electrolyte as an alternative to the commercial organic ones for realizing safer and more reliable, highly performant LIB systems.

DECLARATIONS

Acknowledgments

The authors acknowledge the support by the European Union's Horizon 2020 Research and Innovation Program under grant agreement No. 814464 (Si-DRIVE Project).

Authors' contributions

Investigation, methodology, validation, formal analysis, writing - original draft: Maresca G
Formal analysis and material support: Sankaran A, Santa Maria LJ, Ottaviani M, Fantini S
Supervision, writing- reviewing and editing: Brutti S, Ryan KM
Conceptualization, validation, supervision, writing- reviewing and editing: Appetecchi GB

Availability of data and materials

The authors should declare where the data supporting their findings can be found. Data can be deposited into data repositories or published as Supplementary Material in the journal.

Financial support and sponsorship
This project has received funding from the European Union's Horizon 2020 research and innovation program under grant agreement No. 814464.

Conflicts of interest
All authors declared that there are no conflicts of interest.

Ethical Approval and Consent to Participate
Not applicable.

Consent for Publication
Not applicable.

REFERENCES

1. Armand M, Axmann P, Bresser D, et al. Lithium-ion batteries - current state of the art and anticipated developments. *J Power Sources* 2020;479:228708. DOI
2. Miao Y, Hynan P, von Jouanne A, Yokochi A. Current Li-ion battery technologies in electric vehicles and opportunities for advancements. *Energies* 2019;12:1074. DOI
3. Rangarajan SS, Sunddararaj SP, Sudhakar A, et al. Lithium-ion batteries - the crux of electric vehicles with opportunities and challenges. *Clean Technol* 2022;4:908-30. DOI
4. Gandoman FH, Jaguemont J, Goutam S, et al. Concept of reliability and safety assessment of lithium-ion batteries in electric vehicles: Basics, progress, and challenges. *Appl Energy* 2019;251:113343. DOI
5. Fang C, Wang X, Meng YS. Key issues hindering a practical lithium-metal anode. *Trends Chem* 2019;1:152-8. DOI
6. Feng X, Ouyang M, Liu X, Lu L, Xia Y, He X. Thermal runaway mechanism of lithium ion battery for electric vehicles: a review. *Energy Stor Mater* 2018;10:246-67. DOI
7. Feng X, Ren D, He X, Ouyang M. Mitigating thermal runaway of lithium-ion batteries. *Joule* 2020;4:743-70. DOI
8. Su X, Wu Q, Li J, et al. Silicon-based nanomaterials for lithium-ion batteries: a review. *Adv Energy Mater* 2014;4:1300882. DOI
9. Teki R, Datta MK, Krishnan R, et al. Nanostructured silicon anodes for lithium ion rechargeable batteries. *Small* 2009;5:2236-42. DOI
10. Schwan J, Nava G, Mangolini L. Critical barriers to the large scale commercialization of silicon-containing batteries. *Nanoscale Adv* 2020;2:4368-89. DOI PubMed PMC
11. Chan CK, Peng H, Liu G, et al. High-performance lithium battery anodes using silicon nanowires. *Nat Nanotechnol* 2008;3:31-5. DOI
12. Adenusi H, Chass GA, Passerini S, Tian KV, Chen G. Lithium batteries and the solid electrolyte interphase (SEI) - progress and outlook. *Adv Energy Mater* 2023;13:2203307. DOI
13. Liu Q, Meng T, Yu L, et al. Interface engineering to boost thermal safety of microsized silicon anodes in lithium-ion batteries. *Small Methods* 2022;6:e2200380. DOI
14. Peled E. The electrochemical behavior of alkali and alkaline earth metals in nonaqueous battery systems - the solid electrolyte interphase model. *J Electrochem Soc* 1979;126:2047-51. DOI
15. Peled E, Menkin S. Review - SEI: past, present and future. *J Electrochem Soc* 2017;164:A1703-19. DOI
16. Shin J, Kim T, Lee Y, Cho E. Key functional groups defining the formation of Si anode solid-electrolyte interphase towards high energy density Li-ion batteries. *Energy Stor Mater* 2020;25:764-81. DOI
17. Xu C, Lindgren F, Philippe B, et al. Improved performance of the silicon anode for Li-ion batteries: understanding the surface modification mechanism of fluoroethylene carbonate as an effective electrolyte additive. *Chem Mater* 2015;27:2591-9. DOI
18. Kennedy T, Brandon M, Laffir F, Ryan KM. Understanding the influence of electrolyte additives on the electrochemical performance and morphology evolution of silicon nanowire based lithium-ion battery anodes. *J Power Sources* 2017;359:601-10. DOI
19. Kalhoff J, Eshetu GG, Bresser D, Passerini S. Safer electrolytes for lithium-ion batteries: state of the art and perspectives. *ChemSusChem* 2015;8:2154-75. DOI
20. Krishna DNG, Philip J. Review on surface-characterization applications of X-ray photoelectron spectroscopy (XPS): recent developments and challenges. *Appl Surf Sci Adv* 2022;12:100332. DOI
21. Tan S, Ji YJ, Zhang ZR, Yang Y. Recent progress in research on high-voltage electrolytes for lithium-ion batteries. *Chemphyschem* 2014;15:1956-69. DOI PubMed
22. Xu Z, Yang J, Li H, Nuli Y, Wang J. Electrolytes for advanced lithium ion batteries using silicon-based anodes. *J Mater Chem A* 2019;7:9432-46. DOI

23. Stokes K, Kennedy T, Kim GT, et al. Influence of carbonate-based additives on the electrochemical performance of Si NW anodes cycled in an ionic liquid electrolyte. *Nano Lett* 2020;20:7011-9. DOI
24. Whiteley JM, Kim JW, Piper DM, Lee S. High-capacity and highly reversible silicon-tin hybrid anode for solid-state lithium-ion batteries. *J Electrochem Soc* 2016;163:A251-4. DOI
25. Falco M, Lingua G, Destro M, et al. An electrochemical compatibility investigation of RTIL-based electrolytes with Si-based anodes for advanced Li-ion batteries. *Mater Today Sustain* 2023;21:100299. DOI
26. Bellusci M, Simonetti E, De Francesco M, Appetecchi GB. Ionic liquid electrolytes for safer and more reliable sodium battery systems. *Appl Sci* 2020;10:6323. DOI
27. Montanino M, Alessandrini F, Passerini S, Appetecchi GB. Water-based synthesis of hydrophobic ionic liquids for high-energy electrochemical devices. *Electrochim Acta* 2013;96:124-33. DOI
28. De Francesco M, Simonetti E, Gorgi G, Appetecchi GB. About the purification route of ionic liquid precursors. *Challenges* 2017;8:11. DOI
29. Geaney H, Dickinson C, O'dwyer C, Mullane E, Singh A, Ryan KM. Growth of crystalline copper silicide nanowires in high yield within a high boiling point solvent system. *Chem Mater* 2012;24:4319-25. DOI
30. Stokes K, Geaney H, Sheehan M, Borsa D, Ryan KM. Copper silicide nanowires as hosts for amorphous Si deposition as a route to produce high capacity lithium-ion battery anodes. *Nano Lett* 2019;19:8829-35. DOI PubMed
31. Mullane E, Kennedy T, Geaney H, Dickinson C, Ryan KM. Synthesis of tin catalyzed silicon and germanium nanowires in a solvent-vapor system and optimization of the seed/nanowire interface for dual lithium cycling. *Chem Mater* 2013;25:1816-22. DOI
32. Brutti S, Simonetti E, De Francesco M, et al. Ionic liquid electrolytes for high-voltage, lithium-ion batteries. *J Power Sources* 2020;479:228791. DOI
33. Kim GT, Kennedy T, Brandon M, et al. Behavior of germanium and silicon nanowire anodes with ionic liquid electrolytes. *ACS Nano* 2017;11:5933-43. DOI
34. Zhang W. Lithium insertion/extraction mechanism in alloy anodes for lithium-ion batteries. *J Power Sources* 2011;196:877-85. DOI
35. Ševčík A. Oscillographic polarography with periodical triangular voltage. *Collect Czech Chem Commun* 1948;13:349-77. DOI
36. Randles JEB. A cathode ray polarograph. Part II. - The current-voltage curves. *Trans Faraday Soc* 1948;44:327-38. DOI
37. Ai Q, Li D, Guo J, et al. Artificial solid electrolyte interphase coating to reduce lithium trapping in silicon anode for high performance lithium-ion batteries. *Adv Mater Inter* 2019;6:1901187. DOI
38. de Rooij DMR. Electrochemical methods: fundamentals and applications. *Anti-Corros Methods Mater* 2003:50. DOI
39. Tsierkezos NG. Cyclic voltammetric studies of ferrocene in nonaqueous solvents in the temperature range from 248.15 to 298.15 K. *J Solution Chem* 2007;36:289-302. DOI
40. Kant R. Theory for staircase voltammetry and linear scan voltammetry on fractal electrodes: emergence of anomalous randles-sevik behavior. *Electrochim Acta* 2013;111:223-33. DOI
41. Churikov A, Ivanishchev A, Ivanishcheva I, Sycheva V, Khasanova N, Antipov E. Determination of lithium diffusion coefficient in $LiFePO_4$ electrode by galvanostatic and potentiostatic intermittent titration techniques. *Electrochim Acta* 2010;55:2939-50. DOI
42. Churikov AV, Ivanishchev AV, Ushakov AV, Romanova VO. Diffusion aspects of lithium intercalation as applied to the development of electrode materials for lithium-ion batteries. *J Solid State Electrochem* 2014;18:1425-41. DOI
43. Zeng W, Wang L, Peng X, et al. Enhanced ion conductivity in conducting polymer binder for high-performance silicon anodes in advanced lithium-ion batteries. *Adv Energy Mater* 2018;8:1702314. DOI
44. Sivonxay E, Aykol M, Persson KA. The lithiation process and Li diffusion in amorphous SiO_2 and Si from first-principles. *Electrochim Acta* 2020;331:135344. DOI
45. Wang G, Xu B, Shi J, Wu M, Su H, Ouyang C. New insights into Li diffusion in Li-Si alloys for Si anode materials: role of Si microstructures. *Nanoscale* 2019;11:14042-9. DOI
46. Nakajima T, Groult H. Advanced fluoride-based materials for energy conversion. 2015. Available from: https://www.sciencedirect.com/book/9780128006795/advanced-fluoride-based-materials-for-energy-conversion#book-info [Last accessed on 8 Mar 2024].
47. Macdonald JR, Johnson WB. Fundamentals of impedance spectroscopy. In: Barsoukov E, Macdonald JR, editors. Impedance spectroscopy. Hoboken, NJ: John Wiley & Sons, Inc.; 2018. pp. 1-20. DOI
48. Middlemiss LA, Rennie AJ, Sayers R, West AR. Characterisation of batteries by electrochemical impedance spectroscopy. *Energy Rep* 2020;6:232-41. DOI
49. Barsoukov E, Macdonald JR. Impedance spectroscopy: theory, experiment, and applications. Hoboken, NJ: John Wiley & Sons, Inc.; 2005. DOI
50. Xu W, Flake JC. Composite silicon nanowire anodes for secondary lithium-ion cells. *J Electrochem Soc* 2010;157:A41. DOI
51. Li J, Dahn JR. An in situ X-ray diffraction study of the reaction of Li with crystalline Si. *J Electrochem Soc* 2007;154:A156. DOI
52. Appetecchi G, Shin J, Alessandrini F, Passerini S. 0.6Ah Li/V_2O_5 battery prototypes based on solvent-free PEO-$LiN(SO_2CF_2CF_3)_2$ polymer electrolytes. *J Power Sources* 2005;143:236-42. DOI
53. Appetecchi GB, Passerini S. Poly(ethylene oxide)-$LiN(SO_2CF_2CF_3)_2$ polymer electrolytes: II. Characterization of the interface with lithium. *J Electrochem Soc* 2002;149:A891. DOI
54. Hou T, Yang G, Rajput NN, et al. The influence of FEC on the solvation structure and reduction reaction of $LiPF_6$/EC electrolytes and its implication for solid electrolyte interphase formation. *Nano Energy* 2019;64:103881. DOI
55. Philippe B, Dedryvère R, Gorgoi M, Rensmo H, Gonbeau D, Edström K. Improved performances of nanosilicon electrodes using the salt LiFSI: a photoelectron spectroscopy study. *J Am Chem Soc* 2013;135:9829-42. DOI PubMed
56. Wu Z, Deng L, Li J, et al. Solid electrolyte interphase layer formation on the Si-based electrodes with and without binder studied by

XPS and ToF-SIMS analysis. *Batteries* 2022;8:271. DOI
57. Nakai H, Kubota T, Kita A, Kawashima A. Investigation of the solid electrolyte interphase formed by fluoroethylene carbonate on Si electrodes. *J Electrochem Soc* 2011;158:A798-801. DOI
58. Philippe B, Dedryvère R, Allouche J, et al. Nanosilicon electrodes for lithium-ion batteries: interfacial mechanisms studied by hard and soft X-ray photoelectron spectroscopy. *Chem Mater* 2012;24:1107-15. DOI
59. Morales-ugarte JE, Bolimowska E, Rouault H, Santos-peña J, Santini CC, Benayad A. EIS and XPS investigation on SEI layer formation during first discharge on graphite electrode with a vinylene carbonate doped imidazolium based ionic liquid electrolyte. *J Phys Chem C* 2018;122:18223-30. DOI
60. Piper DM, Evans T, Leung K, et al. Stable silicon-ionic liquid interface for next-generation lithium-ion batteries. *Nat Commun* 2015;6:6230. DOI
61. Forster-tonigold K, Buchner F, Bansmann J, Behm RJ, Groß A. A combined XPS and computational study of the chemical reduction of BMP-TFSI by lithium. *Batteries Supercaps* 2022;5:e202200307. DOI
62. Karimi N, Zarrabeitia M, Geaney H, et al. Stable cycling of Si nanowire electrodes in fluorine-free cyano-based ionic liquid electrolytes enabled by vinylene carbonate as SEI-forming additive. *J Power Sources* 2023;558:232621. DOI
63. Wu J, Ihsan-ul-haq M, Chen Y, Kim J. Understanding solid electrolyte interphases: advanced characterization techniques and theoretical simulations. *Nano Energy* 2021;89:106489. DOI
64. Bhattacharyya S, Hong J, Turban G. Determination of the structure of amorphous nitrogenated carbon films by combined Raman and X-ray photoemission spectroscopy. *J Appl Phys* 1998;83:3917-9. DOI
65. Dementjev A, de Graaf A, van de Sanden M, Maslakov K, Naumkin A, Serov A. X-Ray photoelectron spectroscopy reference data for identification of the C_3N_4 phase in carbon-nitrogen films. *Diam Relat Mater* 2000;9:1904-7. DOI
66. Buchner F, Forster-Tonigold K, Bozorgchenani M, Gross A, Behm RJ. Interaction of a self-assembled ionic liquid layer with graphite(0001): a combined experimental and theoretical study. *J Phys Chem Lett* 2016;7:226-33. DOI PubMed
67. Blyth R, Buqa H, Netzer F, et al. XPS studies of graphite electrode materials for lithium ion batteries. *Appl Surface Sci* 2000;167:99-106. DOI
68. Nguyen CC, Song S. Characterization of SEI layer formed on high performance Si-Cu anode in ionic liquid battery electrolyte. *Electrochem Commun* 2010;12:1593-5. DOI
69. Bhattacharyya S, Cardinaud C, Turban G. Spectroscopic determination of the structure of amorphous nitrogenated carbon films. *J Appl Phys* 1998;83:4491-500. DOI
70. Martin L, Martinez H, Ulldemolins M, Pecquenard B, Le Cras F. Evolution of the Si electrode/electrolyte interface in lithium batteries characterized by XPS and AFM techniques: the influence of vinylene carbonate additive. *Solid State Ion* 2012;215:36-44. DOI
71. Vogl US, Lux SF, Das P, et al. The mechanism of SEI formation on single crystal Si(100), Si(110) and Si(111) electrodes. *J Electrochem Soc* 2015;162:A2281-8. DOI
72. Dedryvère R, Gireaud L, Grugeon S, Laruelle S, Tarascon JM, Gonbeau D. Characterization of lithium alkyl carbonates by X-ray photoelectron spectroscopy: experimental and theoretical study. *J Phys Chem B* 2005;109:15868-75. DOI PubMed
73. Etacheri V, Geiger U, Gofer Y, et al. Exceptional electrochemical performance of Si-nanowires in 1,3-dioxolane solutions: a surface chemical investigation. *Langmuir* 2012;28:6175-84. DOI
74. Dedryvère R, Leroy S, Martinez H, Blanchard F, Lemordant D, Gonbeau D. XPS valence characterization of lithium salts as a tool to study electrode/electrolyte interfaces of Li-ion batteries. *J Phys Chem B* 2006;110:12986-92. DOI PubMed
75. Kim H, Grugeon S, Gachot G, Armand M, Sannier L, Laruelle S. Ethylene bis-carbonates as telltales of SEI and electrolyte health, role of carbonate type and new additives. *Electrochim Acta* 2014;136:157-65. DOI
76. Sharova V, Moretti A, Diemant T, Varzi A, Behm R, Passerini S. Comparative study of imide-based Li salts as electrolyte additives for Li-ion batteries. *J Power Sources* 2018;375:43-52. DOI
77. Eshetu GG, Diemant T, Grugeon S, et al. In-Depth interfacial chemistry and reactivity focused investigation of lithium-imide- and lithium-imidazole-based electrolytes. *ACS Appl Mater Interfaces* 2016;8:16087-100. DOI
78. Leung K, Rempe SB, Foster ME, et al. Modeling electrochemical decomposition of fluoroethylene carbonate on silicon anode surfaces in lithium ion batteries. *J Electrochem Soc* 2014;161:A213-21. DOI
79. Ensling D, Stjerndahl M, Nytén A, Gustafsson T, Thomas JO. A comparative XPS surface study of Li_2FeSiO_4/C cycled with LiTFSI- and $LiPF_6$-based electrolytes. *J Mater Chem* 2009;19:82-8. DOI
80. Nie M, Lucht BL. Role of lithium salt on solid electrolyte interface (SEI) formation and structure in lithium ion batteries. *J Electrochem Soc* 2014;161:A1001-6. DOI
81. Choi N, Yew KH, Lee KY, Sung M, Kim H, Kim S. Effect of fluoroethylene carbonate additive on interfacial properties of silicon thin-film electrode. *J Power Sources* 2006;161:1254-9. DOI
82. Li Q, Liu X, Han X, et al. Identification of the solid electrolyte interface on the Si/C composite anode with FEC as the additive. *ACS Appl Mater Interfaces* 2019;11:14066-75. DOI
83. Bongiorno C, Mannino G, D'alessio U, et al. On the redox activity of the solid electrolyte interphase in the reduction/oxidation of silicon nanoparticles in secondary lithium batteries. *Energy Technol* 2022;10:2100791. DOI